Geomechanics and Engineering, *Vol. 27, No. 4 (2021) 347-359*
https://doi.org/10.12989/gae.2021.27.4.347

Acoustic emission characteristics of marble under uniaxial cyclic loading

Bin Fu and Chun'an Tang*

State Key Laboratory of Coastal and Offshore Engineering, Dalian University of Technology, Dalian 116024, China

(Received May 11, 2020, Revised October 16, 2021, Accepted October 18, 2021)

Abstract. Intractable rock engineering problems encountered in practice are related to the behavior of rocks under different cyclic loadings, the damage evolution of rock subjected to cyclic loading is important for rock engineering design and construction. Three different cyclic loadings were conducted on marble to explore the acoustic emission (AE) parameters evolution during damage. It was found that the continuous decreasing correlation dimension and b value can be deemed as robust signal of the imminent rock failure. The additional cyclic loadings increase the AE events with low energy. The Realistic Failure Process Analysis (RFPA^{2D}) code was implemented to reproduce the AE distribution evolution of the corresponding experiments. Numerical simulations indicate that the AE distribution changes from random to aggregate. The increasing stress leads to the failure mode of sample shifts from shear damage dominated to tensile damage dominant. The additional cyclic loadings increase the number of the shear damage elements.

Keywords: acoustic emission; b value; correlation dimension; uniaxial cyclic compression

1. Introduction

Rock engineering such as underground tunnels, underground energy storage caverns, dam foundations, bridge abutments, etc. (Liu *et al.* 2017). are likely to be subjected to complicated cyclic loadings. Some studies show that rock strength and failure have a close correlation with the complicated loading paths (Cai 2008, Kaiser *et al.* 2001, Sharma *et al.* 1999, Zhu *et al.* 2018). The decreased strength and failure behaviors can be attributed to the complicated loading and unloading as well (Sun *et al.* 2019). Cyclic loading poses a significant hazard on the engineering stability. Hence, considerable efforts have been made to assess the mechanical response of rock under cyclic loadings (Guo *et al.* 2018, He *et al.* 2018, Wang *et al.* 2018, Zhang *et al.* 2017). Meanwhile, it was reported that cyclic loading characteristics such as maximum stress, amplitude, loading waveform and frequency have different damage effects on rock. (Cerfontaine and Collin 2018, Erarslan 2016, Taheri *et al.* 2016). Namely, the failure of rock can be attributed to the accumulative damage caused by different cyclic loadings. Therefore, attentions have been paid to rock damage during cyclic loading as well (Munoz and Taheri 2017, Sun *et al.* 2017, Zhou *et al.* 2017).

Meantime, the damage is closely related to the AE that results from the released strain energy within the materials. Since the discovery of the Kaiser effect in metallic materials (Kaiser 1950), the AE method has been gradually applied to study the rock damage (Goodman 1963). The AE monitoring provides the possibility to investigate the rock damage evolution during the entire failure process without any additional disturbance. Therefore, real-time monitoring of AE events has become an important method for disclosing the evolutionary laws of rock deformation and damage. Numerical experiments on rock AE were conducted and achieved beneficial results (Codeglia *et al.* 2017, Jin *et al.* 2017, Kong *et al.* 2018, Wang *et al.* 2019). Based on the AE characteristics, the rock failure and geotechnical engineering disaster were tried to be predicted (Kim *et al.* 2019, Ma *et al.* 2018, Su *et al.* 2017, Zhang *et al.* 2014). The AE has provided important guidance for the geotechnical engineering (Zhang *et al.* 2015).

However, it is noted that the stress conditions in engineering fields are complicated and frequently encountered with different kinds of cyclic loadings. It is indispensable to investigate AE induced by complicated cyclic stress paths. In this study, three different cyclic loadings are applied on marble to explore the AE characteristics during rock failure. The corresponding numerical simulations are implemented based on RFPA^{2D} to reveal the AE distribution evolution. The effect of the additional cyclic loadings on the rock damage is discussed. The results may play an important role on the further understanding of rock damage under different cyclic loadings and the rock failure prediction.

2. Test program

2.1 Test equipment and test sample

The TAW-2000D electrohydraulic servo test system is used in this experiment. The system is composed of the loading system and the data acquisition system (Fig. 1), which has a load capacity of 2000kN. The force controlled mode is applied in this test. The AE is monitored by the SDAES digital AE detection system which produced by

*Corresponding author, Professor
E-mail: tca@mail.neu.edu.cn

ISSN: 2005-307X (Print), 2092-6219 (Online)

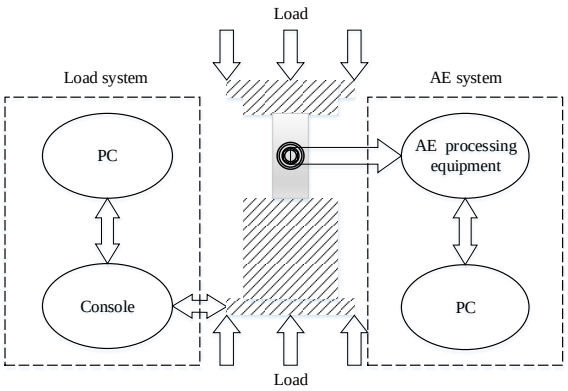

Fig. 1 Experiment system construction framework

Fig. 2 The installation of AE probe

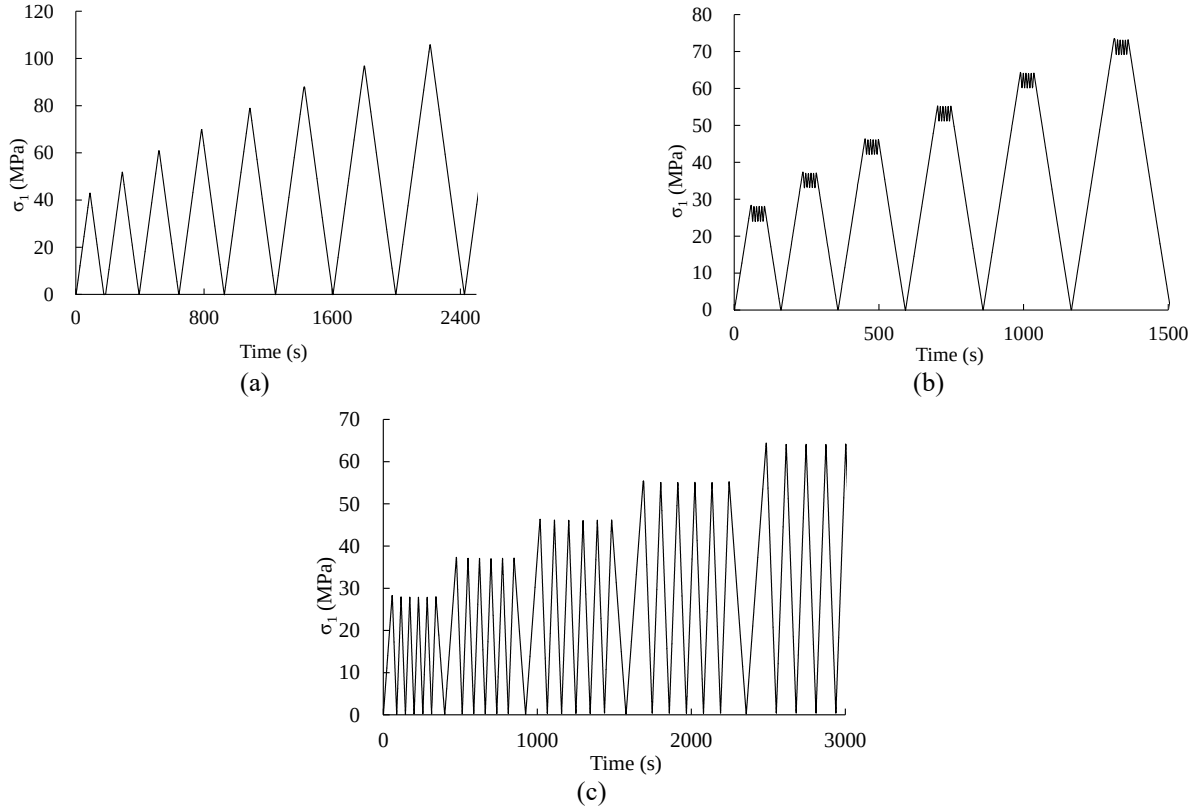

Fig. 3 Different cyclic stress paths: (a) general cyclic loading (b) cycles with 5MPa additional cyclic loadings (c) cycles with large additional cyclic loadings

Beijing Shenghua Technology Co., Ltd. The system consists of four parts: sensor, amplifier, AE acquisition card, and system software. During the test, one DH107 AE probe is used to collect the AE data. The probe is attached on the middle of the rock sample by a rubber band (Fig. 2). To ensure the close contact between the probe and rock sample, couplant is applied for the coupling. To eliminate the effect of environmental noise, the noise of the loading system is tested beforehand and the AE threshold is set up as 40dB. A digital filter is implemented after the preamplifier. The processed signal can be amplified by the main amplifier.

The marble used in this test is collected from a quarry located in Leiyang, China. The Φ50 mm × 100 mm standard rock specimens are prepared according to the ISRM suggested method. The average density and P-wave velocity are measured as 2.8 g/cm^3 and 3600 m/s, respectively. The samples with joint and those density and wave velocity deviate the average value largely are disregarded.

2.2 Test method

Three different kinds of cyclic loading paths are applied on the rock with the same loading rate of 1KN/s. The test cyclic loading paths are provided in Fig. 3. The initial stress is set to be 60% of the uniaxial compressive strength and then increases step-wise in 10MPa until the failure (Fig. 3(a)). To simulate the disturbance encountered in practices, 5MPa additional cyclic loadings and large amplitude additional cyclic loadings that are equal to the cyclic peak stress are applied on the first kind of cyclic loading,

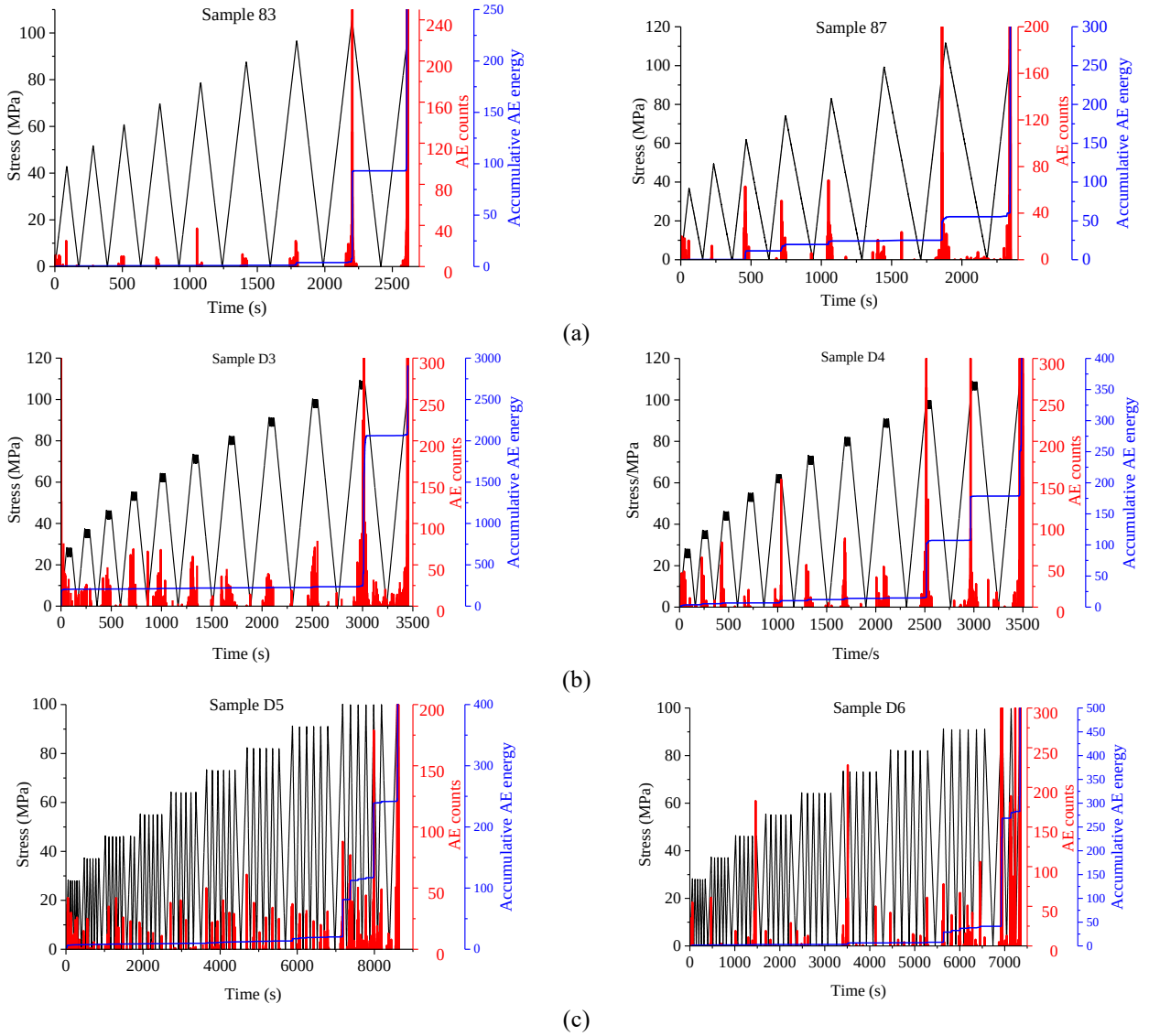

Fig. 4 Evolution of stress, AE counts, and accumulated AE energy with time (a) general cyclic loading (b) cycles with 5MPa additional cyclic loadings (c) cycles with large additional cyclic loadings

respectively (Figs. 3(b)-3(c)). The initial stress is set to be 40% of the uniaxial compressive strength. Two samples were deformed for each type of test.

3. Experimental results

3.1 AE counts and energy

Different samples present similar trend on AE counts and accumulative energy where the AE counts can be divided into three stages (Fig. 4). In the first cycle, the AE is relatively active for different samples. The active AE happens in the second cycle for Sample D3 and D5 as well. The decreasing AE events in the following few cycles indicate that the rock is in the elastic stage (Zhang *et al.* 2015). In this stage, the micro cracks, voids, and joints are further compressed (Xiong *et al.* 2018). However, the low stress is not sufficient to produce much more micro cracks which leads to the rare AE events in this stage. In the third

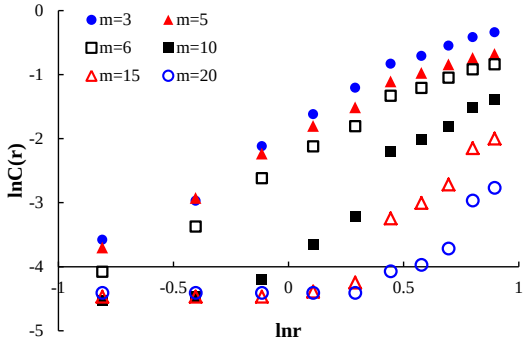

Fig. 5 The effect of m on the variation of ln$C(r)$ and ln$r$

stage, the number of AE events increases as the rock approaches failure.

When additional cyclic loadings applied, the AE events increase significantly (Figs. 4(b)-4(c)). It indicates that small and large additional cyclic loadings both promote the crack development. Furthermore, it shows that the AE

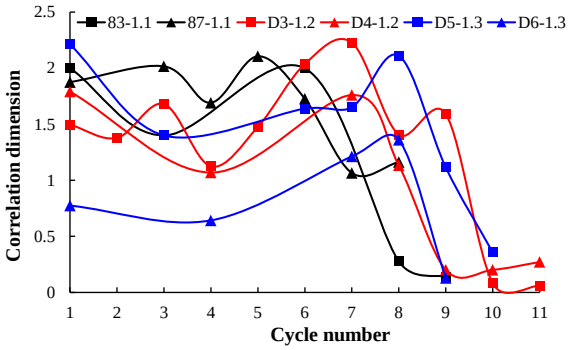

Fig. 6 The variation of correlation dimension with cycle number

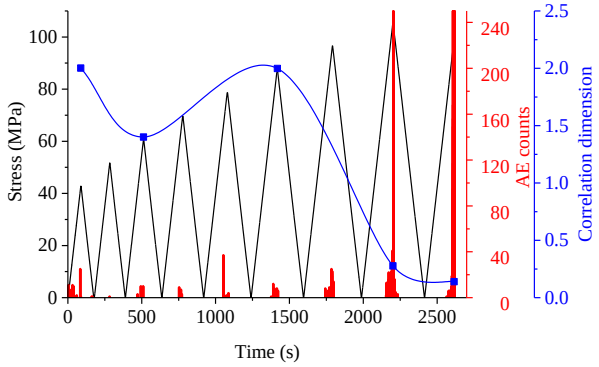

Fig. 7 Comparison on the stress, AE counts, correlation dimension with time of Sample 83

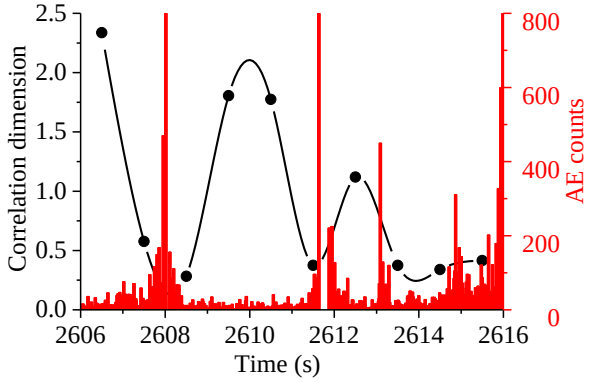

Fig. 8 The variation of the correlation dimension and AE counts in last 10s before the failure of Sample 83

events caused by large additional cyclic loadings are primarily concentrated when the stress of the additional cyclic loading is high. In last one or two cycles, the AE events keep active even when the additional cyclic loadings are low. As the development of the crack, the rock tends to be unstable. On the other hand, the AE energy can be divided into two stages. During the first stage, there is no obvious sharp increment while in last two cycles the accumulative AE energy increases greatly. The energy released in last two cycles is much higher than the accumulation of the former cycles. It indicates that the cracks with high energy are mainly generated in last two cycles. When the additional cyclic loadings applied, this trend has not been changed. The accumulative AE energy released in the former cycles is still far below the energy that released in last two cycles, which suggests that the increased AE events caused by additional cyclic loadings are mainly lower energy.

3.2 Correlation dimension analysis

The correlation dimension estimates the convergence of nearby trajectories of the attractor in the phase space. It reflects the number of independent variables that are necessary to describe the dynamics of the system. Therefore, the correlation dimension can be deemed as a measure of complexity of that being investigated, which belongs to the fractal field of mathematics (Packard *et al.* 1980). The value is closely related to the mechanical behaviors and damages of rock as well (Li *et al.* 2019).

3.2.1 The determination of phase space dimension

When dealing with analytical problems in big data systems, the status variable of the data system should be reconstructed in phase space firstly before the calculation of the chaotic time sequence correlation dimensions (Xie *et al.* 2011). Generally, the method proposed by Grassberger and Procaccia is used to reconstruct phase space to reveal more information (Grassberger and Procaccia 1984). The phase space dimension m is important in the application of the G-P algorithm to determine the correlation dimension. Therefore, the appropriate m should be decided first before the calculation. Different m is applied to calculate the correlation dimension in this test. Fig. 5 shows that $\ln r$ and $\ln C(r)$ present good fitness when m is relatively small. Therefore, m is chosen as 6 in the test due to the higher correlation coefficient.

3.2.2 The variation of the correlation dimension in the whole cycles

Different samples present the similar trend on the correlation dimension. Fig. 6 shows that the correlation dimension can be divided into three stages for all samples. The correlation dimension decreases first and followed by an increasing stage, while when the rock comes to fail the correlation dimension declines sharply. The three-stage trend of the correlation dimension is consistent with the crack development which can be divided into crack closure, crack initiation, start of unstable crack growth. Moreover, it shows that the additional cyclic loadings have little effect on the three-stage trend of the correlation dimension. Sample 83 is taken as an example to illustrate the correlation dimension variation during the whole process (Fig. 7). The inherent micro cracks can be compacted and the rock is in compaction stage in the first cycle (Nicksiar and Martin 2012). The large number of AE events and higher correlation dimension may be contributed to friction between the equipment and rock. The inactive AE and lower correlation dimension in the elastic stage indicates that few new cracks are generated. The increasing peak stress of the cycles activates the AE events again which indicates that the initiation and development of cracks. It leads to the increase of the correlation dimension. In last

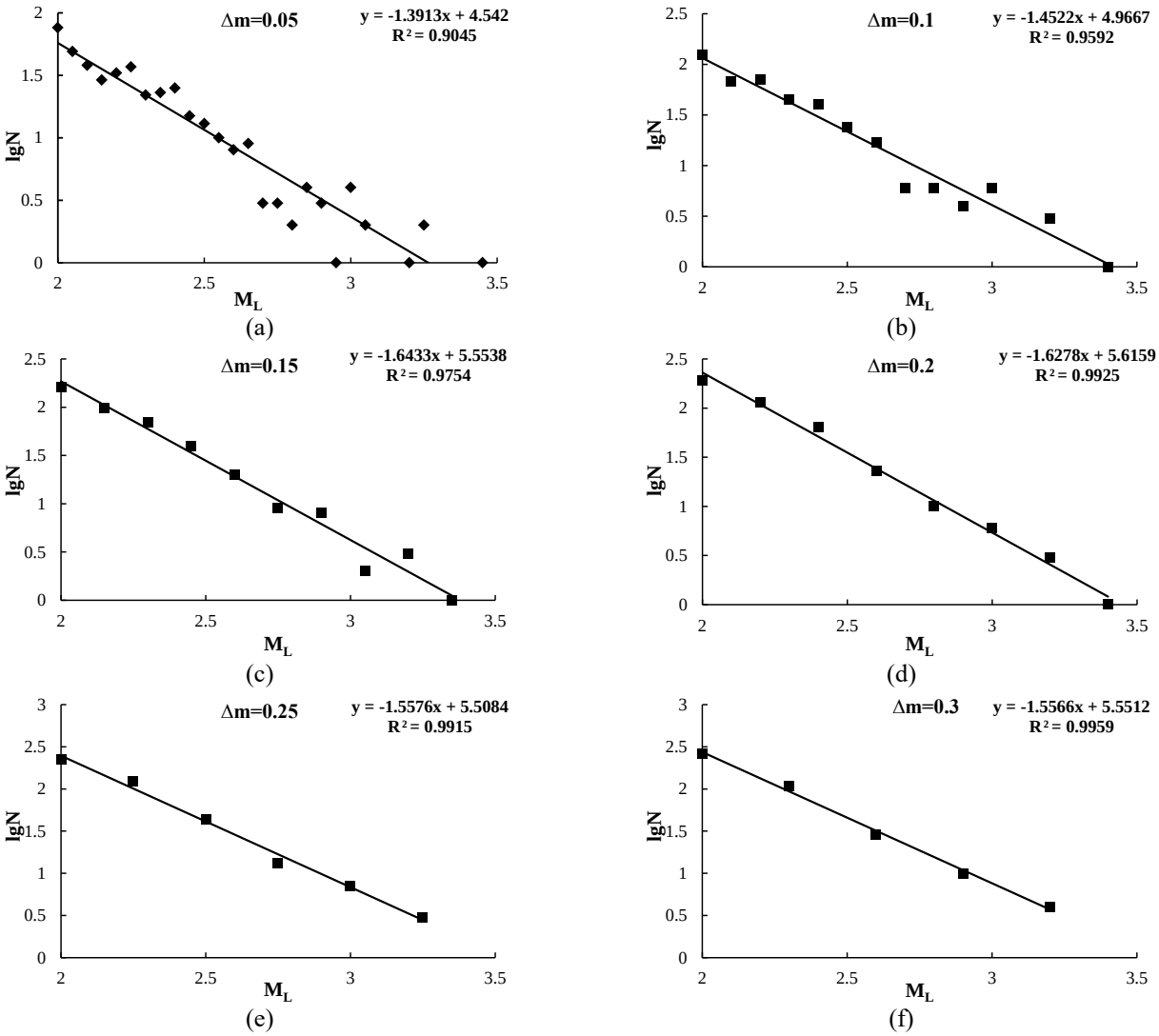

Fig. 9 The determination of b value under different magnitude intervals

two cycles, the generation and coalescence of macro cracks produce large number of AE and the correlation dimension presents a significant decline.

As a typical brittle material, the failure time of rock under uniaxial loading is short. Fig. 4 shows that large number of AE events exist in last one or two cycles as well. Therefore, the correlation dimensions during the final 10s are chosen to investigate as the rock comes to failure. Sample 83 is taken as an example to illustrate. As shown in Fig. 8, the correlation dimension presents a close relationship with the AE counts. The decreasing correlation dimension agrees well with the increasing AE counts while the increasing correlation dimension is consistent with the AE calm period. The macro cracks can be formed before rock failure (Pei *et al.* 2016, Yang *et al.* 2014). The fluctuation of the correlation dimension may be related to the formation of macro cracks with higher AE events. In the last 3s, the correlation dimension keeps low until the rock failure. It indicates that the formation and coalescence of the macro cracks. Namely, the continuous low correlation dimension can be deemed as a signal of the imminent rock failure.

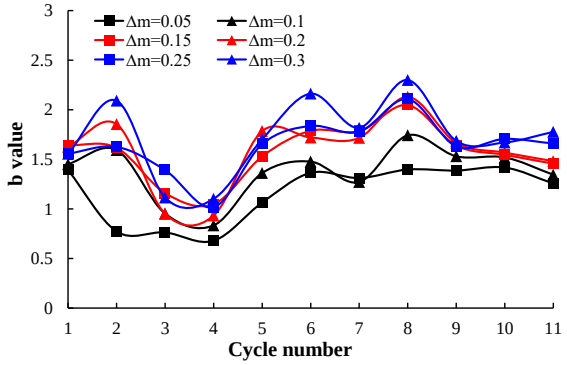

Fig. 10 The variation of the b value with the cycle number under different magnitude intervals

3.3 b value analysis

3.3.1 The calculation of the b value

In the field of earthquake seismology, it is well known that small-magnitude earthquakes occur frequently, whereas large earthquakes occur rarely. Gutenberg and Richter

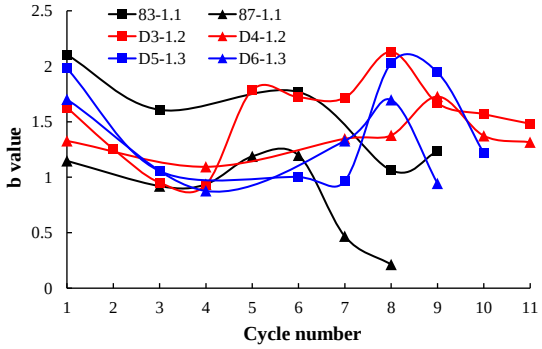

Fig. 11 The variation of the b value with the number of cycles

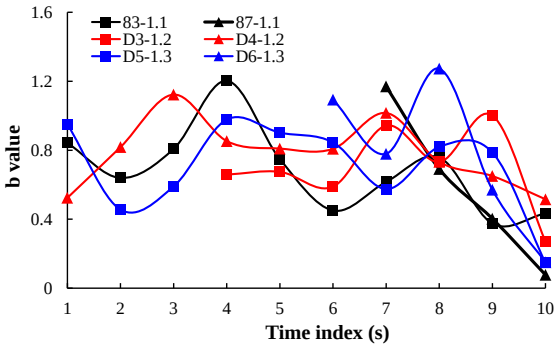

Fig. 12 The variation of the b value in last 10s before the failure

proposed that the slope of the amplitude distribution can be deemed as an effective index to estimate the state of fracturing (Gutenberg and Richter 1936). In the laboratory mechanical experiments on rocks, the monitoring of the AE events follows a remarkable similarity to the cumulative frequency-amplitude relationship observed during earthquakes (Lockner 1993). The b value from the Gutenberg-Richter equation has been widely used to assess the internal damage evolution of rock (Akdag *et al.* 2018, Kim *et al.* 2014, Rodríguez and Celestino 2019). The b value can be obtained by the following equation:

$$\log N = a - bM_L \tag{1}$$

where M_L is the Richter magnitude of earthquakes and it is proportional to the logarithm of the AE amplitude (Rao and Lakshmi 2005), N indicates the incremental frequency (i.e., the number of earthquakes with magnitude greater than M_L), a is constant, and b denotes the b value. Generally, the amplitude of AE is divided by 20 to represent the M_L as shows:

$$M_L = \mathrm{A}/20 \tag{2}$$

To calculate the b value, the log frequency–magnitude graph should be drawn, and its linear trend could be obtained using the least-square method of curve fitting. The b value can be obtained by the negative slope of the log frequency-magnitude.

3.3.2 The determination of magnitude interval

Different magnitude interval can affect the result of b value. The determination of the magnitude interval is the premise to explore the variation of the b value before the calculation. For the same set of data, the calculations of b value for different magnitude interval are shown in Fig. 9. The magnitude interval of M_L is set from 0.05 to 0.3. The number of the point in the figure decreases with the magnitude interval which leads to higher goodness of fit. However, the unconventional data will affect the result significantly when the data point in the figure is small. The large magnitude interval can lead to the two-dimensional data shrink into a single point and the information of the system cannot be presented and analyzed correctly. Otherwise, the smaller magnitude intervals will result in a discrete data distribution in which the lower fitness is not credible.

The variation of b value of the Sample D3 in each cycle calculated by different magnitude intervals is shown in Fig. 10. The b value increases with the magnitude intervals where the 0.05 interval has the lowest value and the 0.3 interval presents the highest value. The b values calculated by different magnitude intervals present similar trend. It seems that the higher interval can produce stable results. However, it should be noted that there are only 5 points in Fig. 9(f) when the magnitude interval is set as 0.3. The increasing interval will reduce the data point in the figure which makes the result incredible. The 0.05 and 0.1 intervals present a little difference with the others. It indicates that the lower interval cannot reveal the system characteristics as well. Therefore, it can be concluded that only when the magnitude interval is within a certain range the effect of the magnitude interval determination on the b trend can be neglected. According to the results above, the magnitude interval is set as 0.2 in this test.

3.3.3 The variation of the b value

The variation of b value with the cycles is shown in Fig. 11. The trend of the b value of different samples is similar and can be divided into three stages. In the first cycle, the b value is relatively higher. Later, the b value decreases first and followed by an increased stage. As the rock approaches failure, the b value presents a decreasing trend again. According to the results of Lei et al. (Lei *et al.* 2000) and Colombo et al (Colombo Ing *et al.* 2003), the decreasing b value indicates the uniformly distributed and the interaction between the cracks. Therefore, it can be deemed that the first decreasing trend of b value may be related to the inactive of AE and later increasing and decreasing b value can be contributed to the generation of AE with small and large amplitude, respectively.

Within the last 10s before rock failure, most of the b value is less than 1.0 and fluctuates within a certain range before the failure (Fig. 12). According to the previous study (Cox and Meredith 1993, Hatton *et al.* 1993), the b value lower than 1.0 denotes the formation of the macro cracks and the failure of the material. Therefore, the figure indicates that the extensive formation of macro crack in last 10s. Meantime, some higher b values suggest the active generation of the micro cracks as well. The higher and lower b values coexist in last 10s. In last 3s, the b value keeps decreasing until failure. The continuous decreasing b

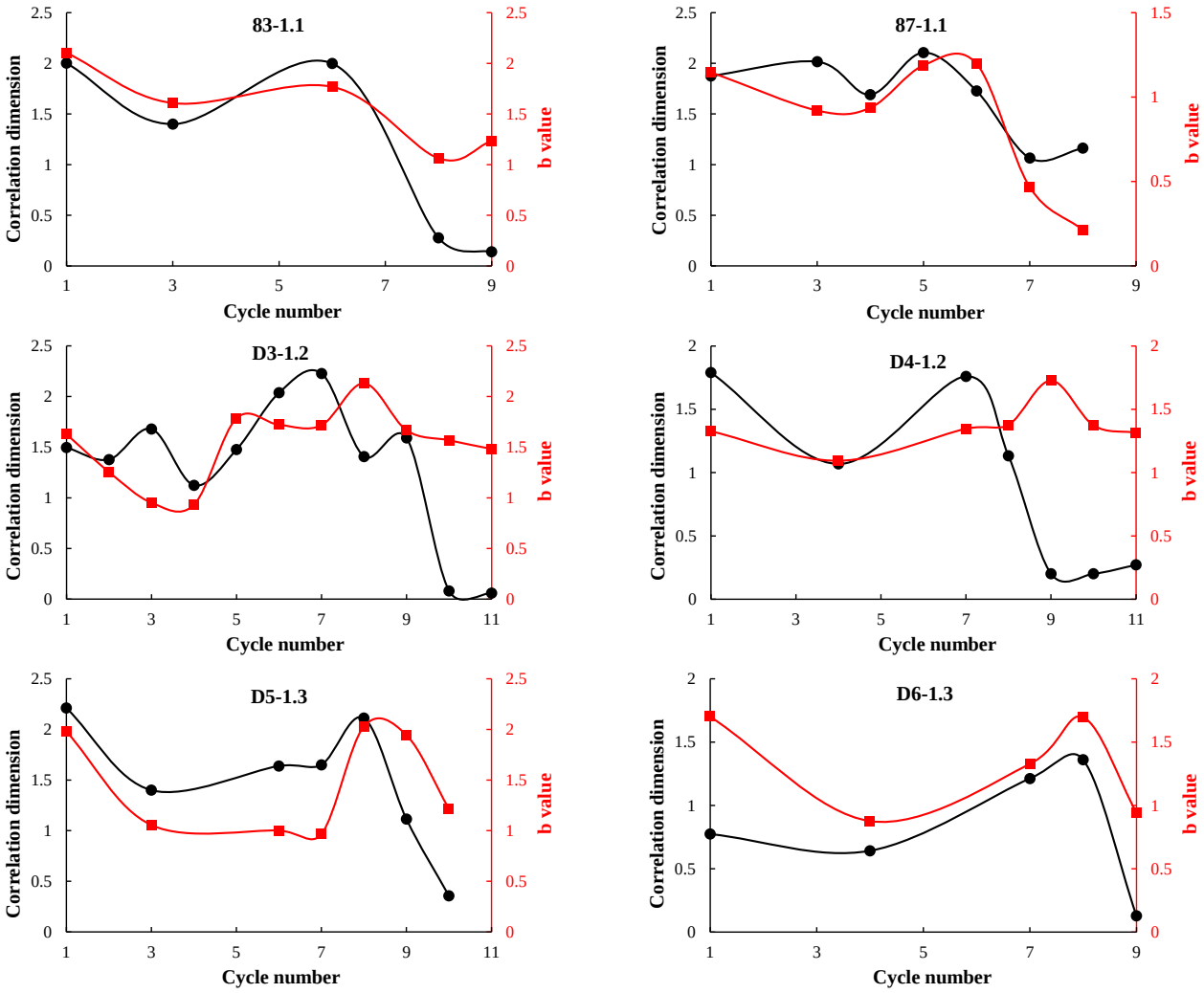

Fig. 13 The variation of the correlation dimension and b value with the cycle number

value denotes the unstable state of the rock and can be deemed as the indication of the imminent rock failure as well. It is noted that the additional cyclic loadings present little influence on the trend. All samples share the same trend on the b value and correlation dimension variation. It suggests that these two parameters are robust to the stress paths, and are closely related to the rock damage and failure prediction.

3.4 The relationship between the correlation dimension and b value

Calculated by different AE sequence, the correlation dimension and b value are both related to the crack development within the rock. Fig. 13 shows that the correlation dimension presents almost simultaneous fluctuations with the b value for different samples. In the initial stage, both the correlation dimension and b value decrease with cycles and followed by an increased stage while they decrease sharply as the rock approaches failure. The continuous decreasing of the correlation dimension and b value can both be deemed as the indication of the imminent failure. The difference is that most of the b values are lower than the correlation dimension in the early stage, while it presents the inverse trend in the later stage. The correlation dimension presents a much more significant decline compared to the b value as the rock approaching failure. It indicates that the correlation dimension is more sensitive to the macro cracks formation.

4. Numerical simulation

The spatial and temporal evolution of AE cannot be obtained by one AE probe in the test. To make up for the shortcomings brought by the experimental equipment, RFPA is employed to reproduce the tests. In RFPA, finite element method is used to calculate and analyze the stress. It assumes that the domain consists of elements with the same shape and size and there is no geometric priority in any orientation. The elements of the rock are assumed to be linear elastic, isotropic and damage-free before loading. The elastic energy stored in the element can be obtained by the stress and strain of the element. Once the element is damaged, all the elastic energy is released in the form of acoustic emission (AE). The rock constitutive relationship and the code details can be found in Tang (1997).

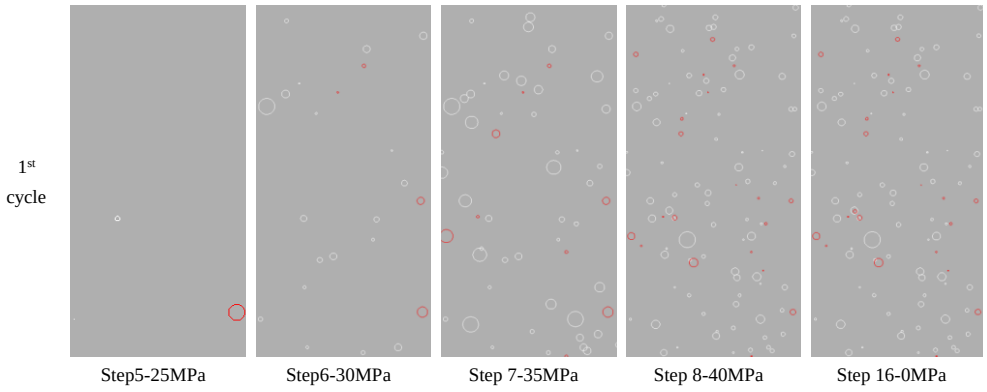

(a)

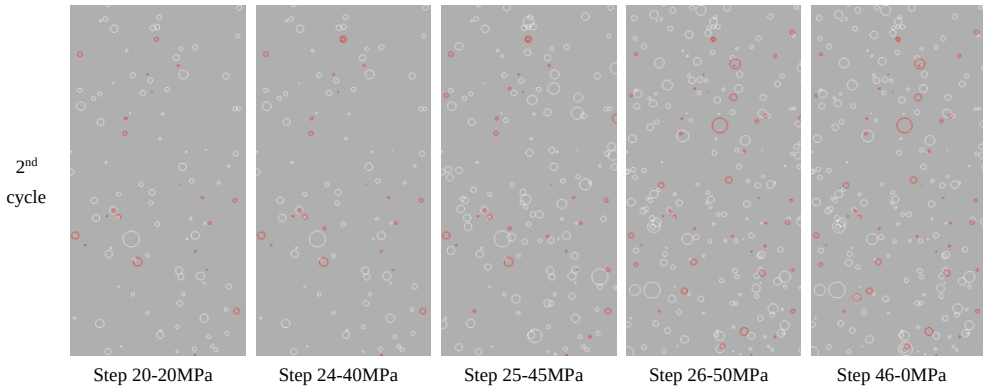

(b)

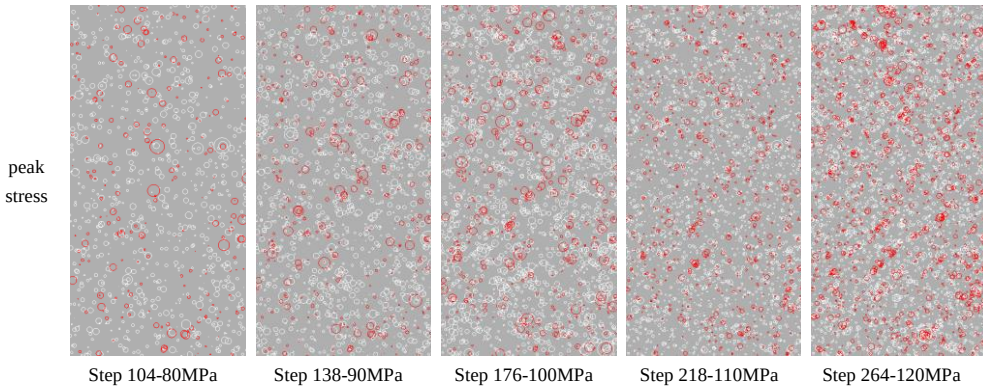

(c)

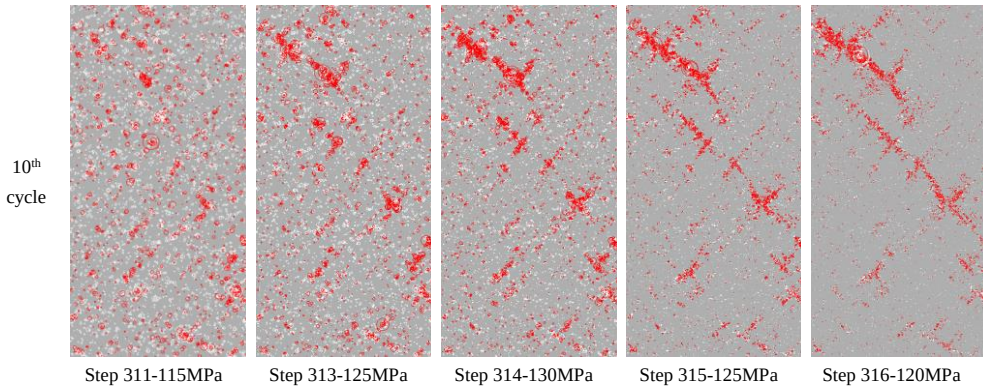

(d)

Fig. 14 AE distribution evolution of sample subjected to the general cyclic loading

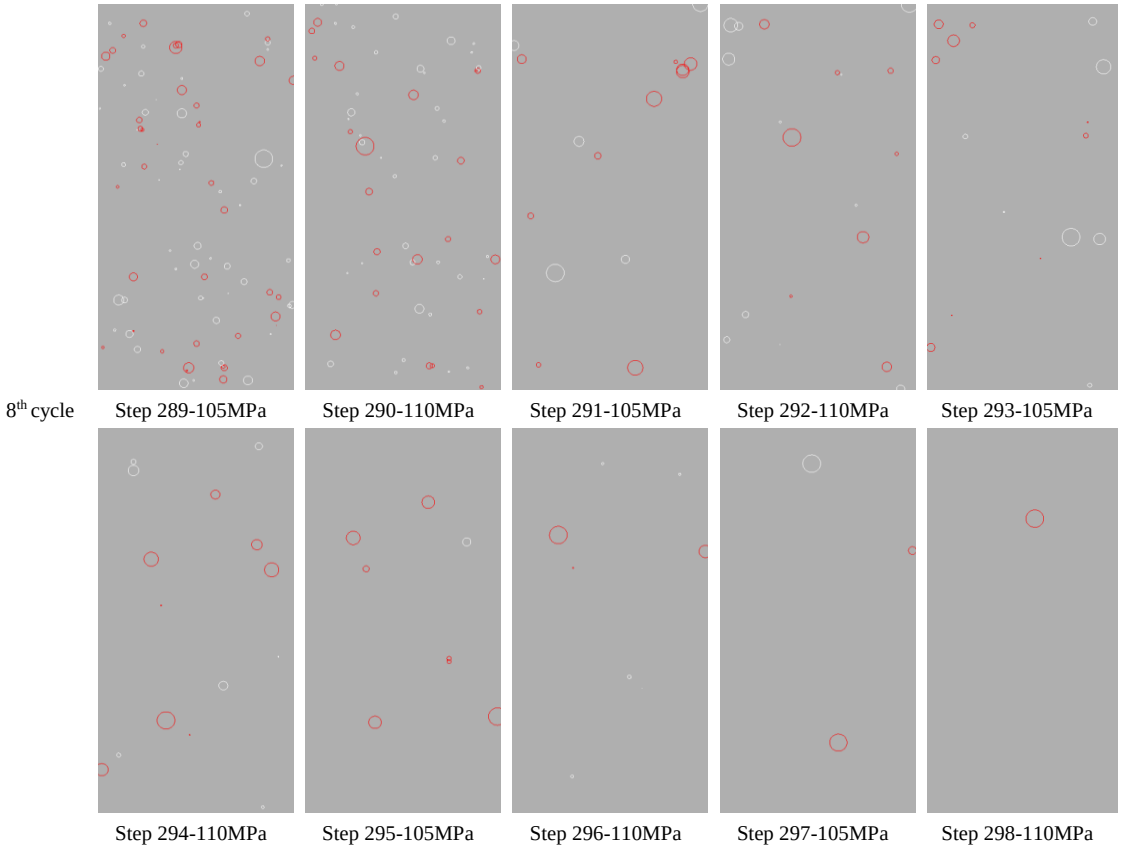

(a)

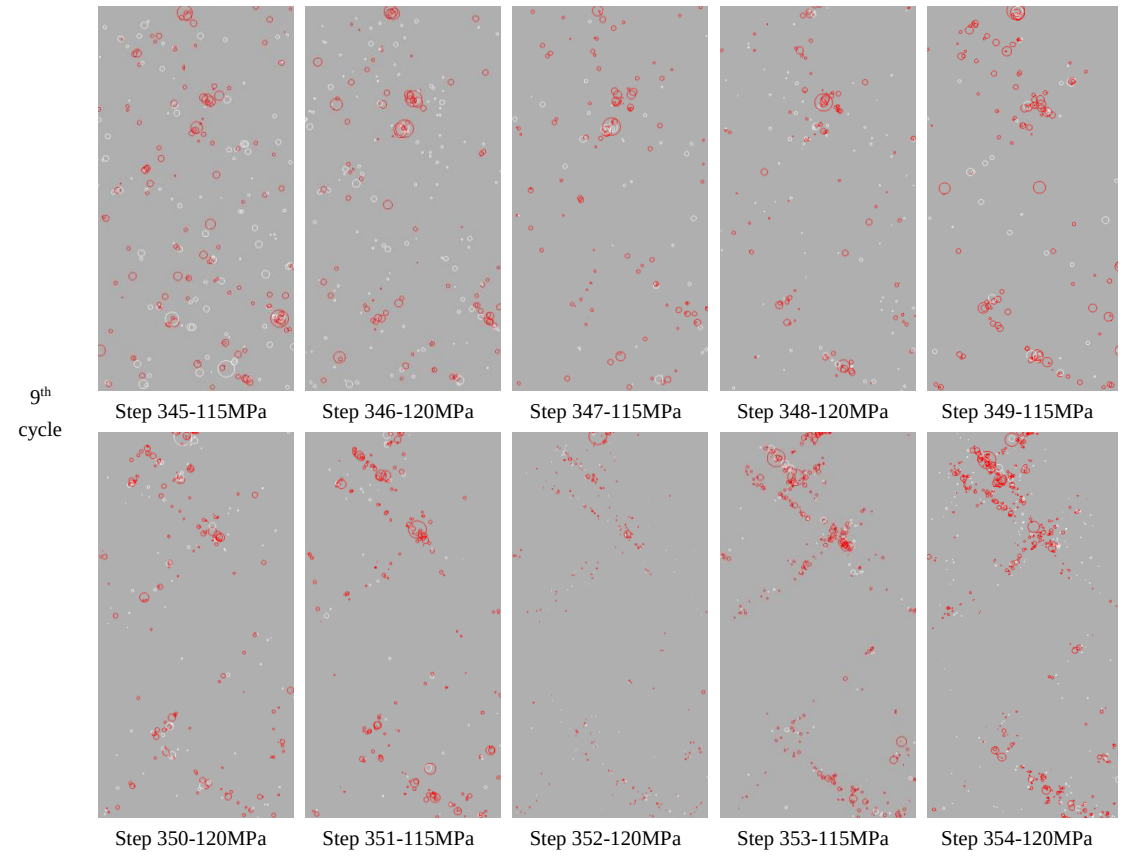

(b)

Fig. 15 AE distribution in current step during the 5MPa additional cyclic loadings

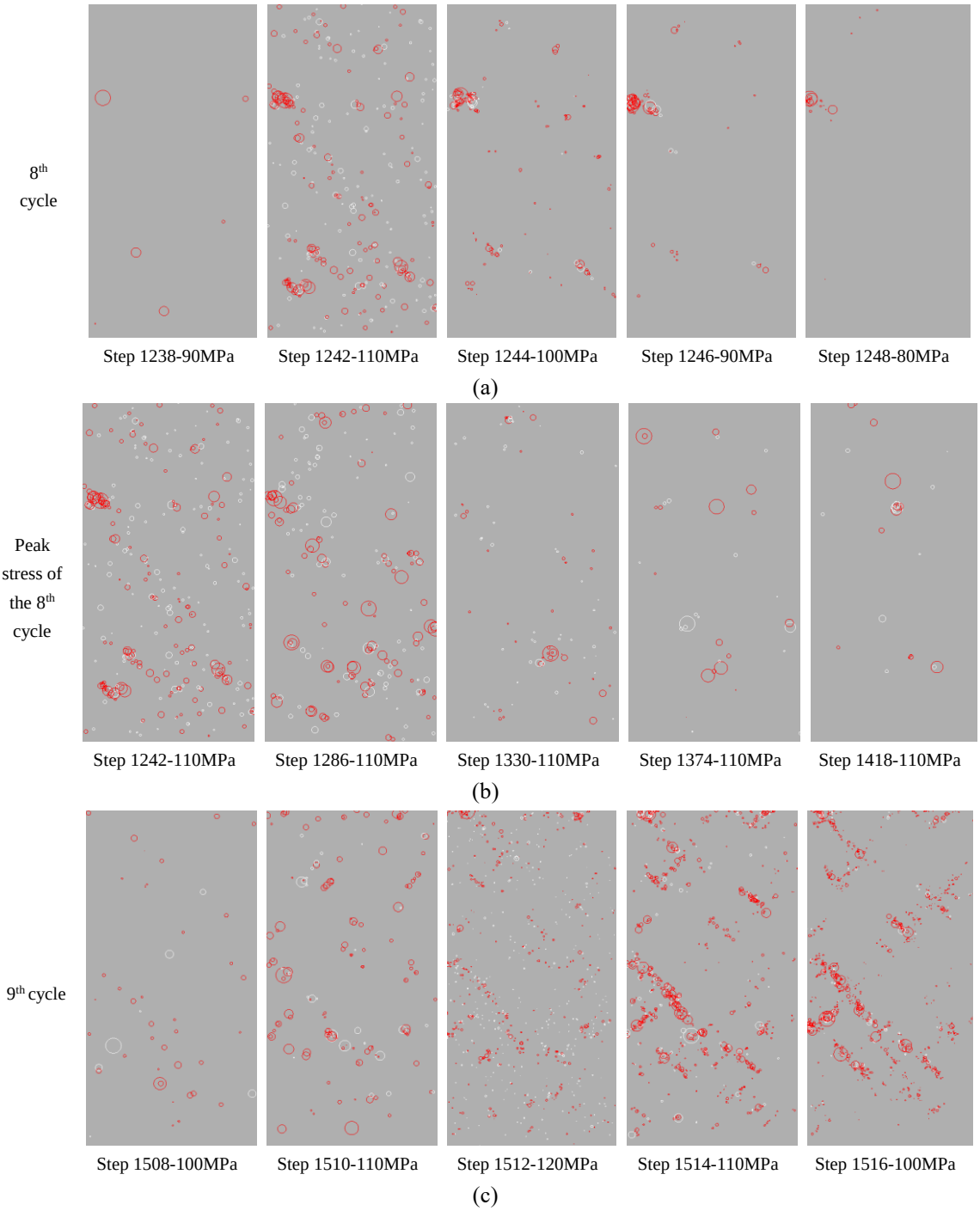

Fig. 16 AE distribution in current step during the large additional cyclic loadings

4.1 Mechanical model and parameters

The corresponding numerical simulations are performed by RFPA^{2D}. The sample is simplified to a plane axisymmetric model of dimensions 50*100 mm^2. A total of 200*400 = 80,000 quadrilateral elements in the same size are employed for meshing the model. The basic parameters of the models are as follows: homogeneity index m = 3; mean elastic modulus = 39.8 GPa; poisson's ratio = 0.27; mean uniaxial compressive strength = 355.8 MPa; ratio of compressive and tensile strength = 10.

4.2 Simulation results

Fig. 14 illustrates the AE distribution evolution of the general cyclic loading. The white and red color cycles in the AE figures represent elements failed in shear and tensile, respectively. The larger the size of the cycles, the higher the energy released when the element is failed. Evident AE events occur when the stress is above 30MPa. The shear failure elements are predominant when the stress is low. The stress increases from 30MPa to 40MPa in the first cycle leads to the increase of AE events, while no element damage occurs in the unloading stage (Fig. 14(a)). In the

second cycle (Fig. 14(b)), rare AE events happen until the stress reaches 40MPa. Once the stress is beyond 40MPa, AE events tend to be active again. In the following cycles, the sample presents similar results with the first two cycles. The AE distributions at the peak stress of each cycle are shown in Fig. 14(c). It indicates that the sample failure shifts from shear dominant to mixed mode of the shear damage and tensile damage. In the 10th cycle (Fig. 14(d)), the lower stress produces large number of AE events and the distribution of the AE begins to gather in certain zones while with tensile damage dominant. The cluster of AE promotes the generation of the macro crack where the sample tends to be unstable and the AE becomes active even during the unloading stage. In Step 315, the tensile damage plays a dominant role while the shear damage is relatively little. During the unloading stage, more and more fractures are coalesced accompanying with a large number of AE events, and two macro cracks formed when the stress decreases to 120MPa.

The additional cyclic loadings cased rare AE events in the early stage compared to the general cyclic loading. Fig. 15 illustrates the AE distribution of the last two cycles when the 5MPa additional cyclic loadings applied. In the 8th cycle (Fig. 15(a)), the AE occurs in every step including the unloading stage. The AE events are mainly induced by tensile damage elements. At the same time, the AE produced by each same additional cycles decrease gradually. It can be concluded that the small additional cyclic loadings caused limited damage to the rock in the early stage. The AE keeps active in the 9th cycle (Fig. 15(b)). The number of AE keeps increasing with the additional cyclic loadings. It suggests that the effect of the small additional cyclic loadings can be divided into two stages. In the first few cycles, the damage that caused by small additional cyclic loadings is little, and the damage decreases with the disturbing cycles. As the increase of the stress, the damage caused by additional cyclic loadings increases significantly and the damage increases with the disturbing cycles.

The large additional cyclic loadings present similar effect with the small additional cyclic loadings. The AE caused by large additional cyclic loadings during the 8th and 9th cycles are shown in Fig. 16. In the 8th additional cyclic loadings (Fig. 16(a)), only when the stress increases to 90MPa, the AE events begin to be reactive. When the stress decreases to 80MPa, only rare AE events occur. The first 7 cycles present similar results where the AE only keeps active when the additional stress is high. The number of AE events produced in each additional cycle decreases gradually until the next additional cyclic loading with higher stress (Fig. 16(b)). In the 9th cycle, the AE distribution shifts from the random to be clustered (Fig. 16(c)). The large additional cyclic loadings produce large number of AE events in the last cycle until the rock failure. The application of large additional cyclic loadings has intensified the rock damage significantly which leads to the failure of the sample eventually.

5. Discussions

Both the experimental and numerical results indicate that the additional cyclic loadings increase the number of AE events greatly. The additional cyclic loadings have certainly intensified the rock damage. The sparse AE distributions in the former additional cycles suggest the lower additional cyclic loading has limited effect on rock damage. As the increase of the peak stress of the additional cyclic loading, the number and the amplitude of AE events presents a corresponding increase. Meantime, the AE induced by the additional cyclic loading of same peak stress decreases with the increasing number of cycles when the stress is low. Only when the peak stress increases to 80% of the sample strength, this downward trend can be changed. The peak stress of the additional cyclic loading affects the AE generation significantly. However, the proportion of accumulated AE energy produced by the additional cyclic loading is low. It seems that the increased AE produced by additional cyclic loading is mainly attributed to the generation of micro cracks with low energy. The additional cyclic loading presents little effect on the macro cracks formation. In terms of the correlation dimension and b value, it shows that samples with different additional cyclic loadings applied present consistent trend with the samples that no additional cyclic loadings applied. It can be inferred that even the additional damage has been induced by the additional cyclic loadings to the rock, the effect is limited and the rock failure model keeps unchanged compared to the general cyclic loading. Therefore, the correlation dimension and b value can be deemed as robust parameters to predict the rock failure even though some disturbance exists.

6. Conclusions

To understand the damage evolution of rock under complex stress environment better, three different cyclic loadings are carried out on marble. The corresponding numerical simulations are conducted based on the RFPA^{2D} code to reproduce the failure process. Detailed damage analyses based on the AE characteristic evolutions are performed. The primary results are as follows:

- Different cyclic loadings present similar trend on the AE counts and accumulative energy. Additional cyclic loadings increase the number of AE events with low energy significantly.
- The correlation dimension and b value present similar trend where the variation can be divided into three stages for all samples. Before the failure of rock, both the correlation dimension and b value declines sharply and the continuous decreasing of the correlation dimension and b value can be deemed as a robust signal of the imminent rock failure.
- Numerical simulations indicate that the increased peak cyclic loading leads to the sample failure mode shifts from shear damage dominated to tensile damage dominated. Additional cyclic loadings increase the number of the shear damage elements.
- The effect of additional cyclic loadings can be mainly attributed to the formation of micro cracks with low energy. The number of AE caused by additional cyclic loading is related to the peak stress of cycles. Additional cyclic loading presents little effect on the rock failure mode.

Acknowledgements

This work was supported by the National Key Research and Development Plan (Grant No. 2018YFC1505301), for which the authors are very grateful.

References

Akdag, S., Karakus, M., Taheri, A., Nguyen, G. and Manchao, H. (2018), "Effects of thermal damage on strain burst mechanism for brittle rocks under true-triaxial loading conditions", *Rock Mech. Rock Eng.*, **51**(6), 1657-1682. https://doi.org/10.1007/s00603-018-1415-3.

Cai, M. (2008), "Influence of stress path on tunnel excavation response – Numerical tool selection and modeling strategy", *Tunn. Undergr. Sp. Tech*, **23**(6), 618-628. https://doi.org/10.1016/j.tust.2007.11.005.

Cerfontaine, B. and Collin, F. (2018), "Cyclic and fatigue behaviour of rock materials: Review, interpretation and research perspectives", *Rock Mech. Rock Eng.*, **51**(2), 391-414. https://doi.org/10.1007/s00603-017-1337-5.

Codeglia, D., Dixon, N., Fowmes, G.J. and Marcato, G. (2017), "Analysis of acoustic emission patterns for monitoring of rock slope deformation mechanisms", *Eng. Geol.*, **219**(Mar), 21-31. https://doi.org/10.1016/j.enggeo.2016.11.021.

Colombo Ing, S., Main, I.G. and Forde, M.C. (2003), "Assessing damage of reinforced concrete beam using 'b-value' analysis of acoustic emission signals", *J. Mater. Civil. Eng.*, **15**(3), 280-286. https://doi.org/10.1061/(ASCE)0899-1561(2003)15:3(280).

Cox, S.J.D. and Meredith, P.G. (1993), "Microcrack formation and material softening in rock measured by monitoring acoustic emissions", *Int. J. Rock Mech. Min. Sci. Geomech. Abstr.*, **30**(1), 11-24. https://doi.org/10.1016/0148-9062(93)90172-a.

Erarslan, N. (2016), "Microstructural investigation of subcritical crack propagation and Fracture Process Zone (FPZ) by the reduction of rock fracture toughness under cyclic loading", *Eng. Geol.*, **208**(Jun), 181-190. https://doi.org/10.1016/j.enggeo.2016.04.035.

Goodman, R.E. (1963), "Subaudible noise during compression of rocks", *Geol. Soc. Am. Bull.*, **74**(4), 487. https://doi.org/10.1130/0016-7606(1963)74[487:Sndcor]2.0.Co;2.

Grassberger, P. and Procaccia, I. (1984), "Dimensions and entropies of strange attractors from a fluctuating dynamics approach", *Physica D*, **13**(1), 34-54. https://doi.org/10.1016/0167-2789(84)90269-0.

Guo, H.J., Ji, M., Zhang, Y.D. and Zhang, M. (2018), "Study of mechanical property of rock under uniaxial cyclic loading and unloading", *Adv. Civ. Eng.* https://doi.org/10.1155/2018/1670180.

Gutenberg, B. and Richter, C.F. (1936), "Magnitude and energy of earthquakes", *Science (New York, N.Y.)*, **83**(2147), 183-185. https://doi.org/10.1126/science.83.2147.183.

Hatton, C.G., Main, I.G. and Meredith, P.G. (1993), "A comparison of seismic and structural measurements of scaling exponents during tensile subcritical crack-growth", *J. Struct. Geol.*, **15**(12), 1485-1495. https://doi.org/10.1016/0191-8141(93)90008-x.

He, M.M., Huang, B.Q., Zhu, C.H., Chen, Y.S. and Li, N. (2018), "Energy dissipation-based method for fatigue life prediction of rock salt", *Rock Mech. Rock Eng.*, **51**(5), 1447-1455. https://doi.org/10.1007/s00603-018-1402-8.

Jin, P., Wang, E. and Song, D. (2017), "Study on correlation of acoustic emission and plastic strain based on coal-rock damage theory", *Geomech. Eng.*, **12**(4), 627-637. https://doi.org/10.12989/gae.2017.12.4.627.

Kaiser, E.J. (1950), "A study of acoustic phenomena in tensile test", Ph.D. Dissertation, Technical University of Munich, Munich.

Kaiser, P.K., Yazici, S. and Maloney, S. (2001), "Mining-induced stress change and consequences of stress path on excavation stability–A case study", *Int. J. Rock Mech. Min. Sci.*, **38**(2), 167-180. https://doi.org/10.1016/S1365-1609(00)00038-1.

Kim, J.-S., Kim, G.-Y., Baik, M.-H., Finsterle, S. and Cho, G.-C. (2019), "A new approach for quantitative damage assessment of in-situ rock mass by acoustic emission", *Geomech. Eng.*, **18**(1), 11-20. https://doi.org/10.12989/gae.2019.18.1.011.

Kim, J.S., Lee, K.S., Cho, W.J., Choi, H.J. and Cho, G.C. (2014), "A comparative evaluation of stress–strain and acoustic emission methods for quantitative damage assessments of brittle rock", *Rock Mech. Rock Eng.*, **48**(2), 495-508. https://doi.org/10.1007/s00603-014-0590-0.

Kong, B., Wang, E. and Li, Z. (2018), "Regularity and coupling correlation between acoustic emission and electromagnetic radiation during rock heating process", *Geomech. Eng.*, **15**(5), 1125-1133. https://doi.org/10.12989/gae.2018.15.5.1125.

Lei, X.L., Kusunose, K., Rao, M., Nishizawa, O. and Satoh, T. (2000), "Quasi-static fault growth and cracking in homogeneous brittle rock under triaxial compression using acoustic emission monitoring", *J. Geophys. Res.-Sol. Ea.*, **105**(B3), 6127-6139. https://doi.org/10.1029/1999jb900385.

Li, D.X., Wang, E.Y., Kong, X.G., Ali, M. and Wang, D.M. (2019), "Mechanical behaviors and acoustic emission fractal characteristics of coal specimens with a pre-existing flaw of various inclinations under uniaxial compression", *Int. J. Rock Mech. Min. Sci.*, **116**(Apr), 38-51. https://doi.org/10.1016/j.ijrmms.2019.03.022.

Liu, Y., Dai, F., Fan, P.X., Xu, N.W. and Dong, L. (2017), "Experimental investigation of the influence of joint geometric configurations on the mechanical properties of intermittent jointed rock models under cyclic uniaxial compression", *Rock Mech. Rock Eng.*, **50**(6), 1453-1471. https://doi.org/10.1007/s00603-017-1190-6.

Lockner, D. (1993), "The role of acoustic emission in the study of rock fracture", *Int. J. Rock Mech. Min. Sci. Geomech. Abstr.*, **30**(7), 883-899. https://doi.org/10.1016/0148-9062(93)90041-B.

Ma, T.H., Tang, C.A., Tang, S.B., Kuang, L., Yu, Q., Kong, D.Q. and Zhu, X. (2018), "Rockburst mechanism and prediction based on microseismic monitoring", *Int. J. Rock Mech. Min. Sci.*, **110**(Oct), 177-188. https://doi.org/10.1016/j.ijrmms.2018.07.016.

Munoz, H. and Taheri, A. (2017), "Local damage and progressive localisation in porous sandstone during cyclic loading", *Rock Mech. Rock Eng.*, **50**(12), 3253-3259. https://doi.org/10.1007/s00603-017-1298-8.

Nicksiar, M. and Martin, C.D. (2012), "Evaluation of methods for determining crack initiation in compression tests on low-porosity rocks", *Rock Mech. Rock Eng.*, **45**(4), 607-617. https://doi.org/10.1007/s00603-012-0221-6.

Packard, N.H., Crutchfield, J.P., Farmer, J.D. and Shaw, R.S. (1980), "Geometry from a time-series", *Phys. Rev. Lett.*, **45**(9), 712-716. https://doi.org/10.1103/PhysRevLett.45.712.

Pei, J., Fei, W. and Liu, J. (2016), "Spatial evolution and fractal characteristics of natural fractures in marbles under uniaxial compression loading based on the source location technology of acoustic emission", *Environ. Earth Sci.*, **75**(9), 828. https://doi.org/10.1007/s12665-016-5649-7.

Rao, M. and Lakshmi, K.J.P. (2005), "Analysis of b-value and improved b-value of acoustic emissions accompanying rock fracture", *Curr. Sci. India*, **89**(9), 1577-1582. https://www.jstor.org/stable/24110936.

Rodríguez, P. and Celestino, T.B. (2019), "Application of acoustic emission monitoring and signal analysis to the qualitative and quantitative characterization of the fracturing process in rocks",

Eng. Fract. Mech., **210**(1), 54-69. https://doi.org/10.1016/j.engfracmech.2018.06.027.

Sharma, J.S., Chu, J. and Zhao, J. (1999), "Geological and geotechnical features of Singapore: an overview", *Tunn. Undergr. Sp. Tech*, **14**(4), 419-431. https://doi.org/10.1016/s0886-7798(00)00005-5.

Su, F.Q., Itakura, K.I., Deguchi, G. and Ohga, K. (2017), "Monitoring of coal fracturing in underground coal gasification by acoustic emission techniques", *Appl. Energ.*, **189**, 142-156. https://doi.org/10.1016/j.apenergy.2016.11.082.

Sun, B., Zhu, Z.D., Shi, C. and Luo, Z.H. (2017), "Dynamic mechanical behavior and fatigue damage evolution of sandstone under cyclic loading", *Int. J. Rock Mech. Min. Sci.*, **94**, 82-89. https://doi.org/10.1016/j.ijrmms.2017.03.003.

Sun, H., Liu, X.L. and Zhu, J.B. (2019), "Correlational fractal characterisation of stress and acoustic emission during coal and rock failure under multilevel dynamic loading", *Int. J. Rock Mech. Min. Sci.*, **117**(May), 1-10. https://doi.org/10.1016/j.ijrmms.2019.03.002.

Taheri, A., Yfantidis, N., Olivares, C.L., Connelly, B.J. and Bastian, T.J. (2016), "Experimental study on degradation of mechanical properties of sandstone under different cyclic loadings", *Geotech. Test. J.*, **39**(4), 673-687. https://doi.org/10.1520/gtj20150231.

Tang, C.A. (1997), "Numerical simulation of progressive rock failure and associated seismicity", *Int. J. Rock Mech. Min. Sci.*, **34**(2), 249. https://doi.org/10.1016/s0148-9062(96)00039-3.

Wang, Q.S., Chen, J.X., Guo, J.Q., Luo, Y.B., Wang, H.Y. and Liu, Q. (2019), "Acoustic emission characteristics and energy mechanism in karst limestone failure under uniaxial and triaxial compression", *Bull. Eng. Geol. Environ.*, **78**(3), 1427-1442. https://doi.org/10.1007/s10064-017-1189-y.

Wang, Z.L., Yao, J.K., Tian, N.C., Zheng, J.B. and Gao, P. (2018), "Mechanical behavior and damage evolution for granite subjected to cyclic loading", *Adv. Mater. Sci. Eng.* https://doi.org/10.1155/2018/4312494.

Xie, H.P., Liu, J.F., Ju, Y., Li, J. and Xie, L.Z. (2011), "Fractal property of spatial distribution of acoustic emissions during the failure process of bedded rock salt", *Int. J. Rock Mech. Min. Sci.*, **48**(8), 1344-1351. https://doi.org/10.1016/j.ijrmms.2011.09.014.

Xiong, L.F., Wu, S.C. and Zhang, S.H. (2018), "Mechanical behavior of a granite from wuyi mountain: Insights from strain-based approaches", *Rock Mech. Rock Eng.*, **52**(3), 719-736. https://doi.org/10.1007/s00603-018-1617-8.

Yang, S.-q., Ni, H.-m. and Wen, S. (2014), "Spatial acoustic emission evolution of red sandstone during multi-stage triaxial deformation", *J. Cent. South. Univ.*, **21**(8), 3316-3326. https://doi.org/10.1007/s11771-014-2305-9.

Zhang, C.D., Liang, W.G., Li, Z.G., Xu, S.G. and Zhao, Y.S. (2015), "Observations of acoustic emission of three salt rocks under uniaxial compression", *Int. J. Rock Mech. Min. Sci.*, **77**(C), 19-26. https://doi.org/10.1016/j.ijrmms.2015.03.030.

Zhang, Y., Chen, Y.L., Yu, R.G., Hu, L.Q. and Irfan, M. (2017), "Effect of loading rate on the felicity effect of three rock types", *Rock Mech. Rock Eng.*, **50**(6), 1673-1681. https://doi.org/10.1007/s00603-017-1178-2.

Zhang, Z.Z., Gao, F. and Shang, X.J. (2014), "Rock burst proneness prediction by acoustic emission test during rock deformation", *J. Cent. South. Univ.*, **21**(1), 373-380. https://doi.org/10.1007/s11771-014-1950-3.

Zhou, S.W., Xia, C.C., Zhao, H.B., Mei, S.H. and Zhou, Y. (2017), "Statistical damage constitutive model for rocks subjected to cyclic stress and cyclic temperature", *Acta Geophys.*, **65**(5), 893-906. https://doi.org/10.1007/s11600-017-0073-2.

Zhu, J.B., Zhou, T., Liao, Z.Y., Sun, L., Li, X.B. and Chen, R. (2018), "Replication of internal defects and investigation of mechanical and fracture behaviour of rock using 3D printing and 3D numerical methods in combination with X-ray computerized tomography", *Int. J. Rock Mech. Min. Sci.*, **106**(Jun), 198-212. https://doi.org/10.1016/j.ijrmms.2018.04.022.

GC